DNA and other biopolymers at unprecedented speeds. Using electrophysiology techniques[8,21], we tested one of our robust, electrically quiet, 5-nm-diameter pores with double-stranded DNA. After applying a voltage bias that would draw the negatively charged DNA molecules through the nanopore, we observed diminutions of the ionic current (Fig. 5), reminiscent of the ionic-current blockages observed when single strands of DNA are translocated through the channel formed by α-haemolysin in a lipid bilayer[22,23]. Because no such blockages were seen during one hour of monitoring before adding DNA, and because the blockages ceased when the voltage bias was reversed, we attribute these blockages to interactions of individual DNA molecules with the nanopore. The duration of these blockades was on the order of milliseconds, and they consistently exhibited current reductions to 88% of the open-pore value. This last value is commensurate with translocation of a rod-like molecule whose cross-sectional area is 3–4 nm^2 (ref. 24).

The experimental observations, model considerations and the demonstration of an electronic device show that ion-beam sculpting represents a promising new approach to nanoscale fabrication. With feedback control, reproducibility does not depend on precisely matching all conditions and starting dimensions. The method should be useful for fabricating a variety of nanoscale semiconductor devices, as similar sculpting phenomena have been observed for geometries such as thin slits, trenches and crosses, in several materials, like SiO_2, Si and Al. Furthermore, next-generation ion-source arrays and mask technologies (see http://www-afrd.lbl.gov/ ibt.html) combined with multichannel ion detectors will allow highly parallel applications of nanoscale ion sculpting methods. □

1. Ito, T. & Okazaki, S. Pushing the limits of lithography. *Nature* **406,** 1027–1031 (2000).
2. Joachim, C., Gimzewski, J. K. & Aviram, A. Electronics using hybrid-molecular and mono-molecular devices. *Nature* **408,** 541–548 (2000).
3. Stupp, S. I. & Braun, P. V. Molecular manipulation of microstructures: Biomaterials, ceramics, and semiconductors. *Science* **277,** 1242–1248 (1997).
4. Reed, M. A., Zhou, C., Deshpande, M. R. & Muller, C. J. The electrical measurement of molecular junctions. *Ann. NY Acad. Sci.* **852,** 133–144 (1998).
5. Zhou, C., Deshpande, M. R. & Reed, M. A. Nanoscale metal/self-assembled monolayer/metal heterostructures. *Appl. Phys. Lett.* **71,** 611–613 (1997).
6. Ralph, D. C., Black, C. T. & Tinkham, M. Spectroscopic measurements of discrete electronic states in single metal particles. *Phys. Rev. Lett.* **74,** 3241–3244 (1995).
7. Deshmukh, M. M., Ralph, D. C., Thomas, M. & Silcox, J. Nanofabrication using a stencil mask. *Appl. Phys. Lett.* **75,** 1631–1633 (1999).
8. Hille, B. *Ionic Channels and Excitable Membranes* (Sinauer, Sunderland, Massachusetts, 1992).
9. Johnson, R. E. & Shou, J. Sputtering of inorganic insulators. *K. Danske Vidensk. Selsk. Mat.-fys. Meddr.* **43,** 403–494 (1993).
10. Sigmund, P. Introduction to sputtering. *K. Danske Vidensk. Selsk. Mat.-fys. Meddr.* **43,** 7–26 (1993).
11. Nenandovic, T., Perraillon, B., Bogdanov, Z., Djordjevic, Z. & Milic, M. Sputtering and surface topography of oxides. *Nucl. Instrum. Methods B* **48,** 538–543 (1990).
12. Gnaser, H. *Ion Irradiation of Solid Surfaces* (Springer, Berlin/Heidelberg, New York, 1999).
13. Mayer, T. M., Chason, E. & Howard, A. J. Roughening instability and ion-induced viscous relaxation of SiO_2 surfaces. *J. Appl. Phys.* **76,** 1633–1643 (1994).
14. Carter, G. Viscoelastic buckling and plastic-flow deterministic mechanistic mechanisms for ripple initiation on ion bombarded amorphous solids. *Surf. Interf. Anal.* **25,** 952–954 (1997).
15. Brongersma, M. L., Snoeks, E., Dillen, T. V. & Polman, A. Origin of MeV ion irradiation-induced stress changes in SiO_2. *J. Appl. Phys.* **88,** 59–64 (2000).
16. Erlebacher, J., Aziz, M. J., Chason, E., Sinclair, M. B. & Floro, J. A. Spontaneous pattern formation on ion bombarded Si(001). *Phys. Rev. Lett.* **82,** 2330–2333 (1999).
17. Erlebacher, J., Aziz, M. J., Chason, E. & Aziz, M. J. Nonlinear amplitude evolution during spontaneous patterning of ion-bombarded Si(001). *J. Vacuum Sci. Technol. A* **18,** 115–120 (2000).
18. Kasianowicz, J., Brandin, E., Branton, D. & Deamer, D. W. Characterization of individual polynucleotide molecules using a membrane channel. *Proc. Natl Acad. Sci. USA* **93,** 13770–13773 (1996).
19. Bezrukov, S. M., Vodyanoy, I. & Parsegian, V. A. Counting polymers moving through a single ion channel. *Nature* **370,** 279–281 (1994).
20. Gu, L. Q., Braha, O., Conlan, S., Cheley, S. & Bayley, H. Stochastic sensing of organic analytes by a pore-forming protein containing a molecular adaptor. *Nature* **398,** 686–690 (1999).
21. Hammill, O. P., Marty, A., Neher, E., Sakmann, B. & Sigworth, F. J. Improved patch-clamp techniques for high-resolution current recording from cells and cell-free membrane patches. *Eur. J. Physiol.* **391,** 85–100 (1981).
22. Akeson, M., Branton, D., Kasianowicz, J. J., Brandin, E. & Deamer, D. W. Microsecond time-scale discrimination among polycytidylic acid, polyadenylic acid, and polyuridylic acid as homopolymers or as segments within single RNA molecules. *Biophys. J.* **77,** 3227–3233 (1999).
23. Meller, A., Nivon, L., Brandin, E., Golovchenko, J. & Branton, D. Rapid nanopore discrimination between single polynucleotide molecules. *Proc. Natl Acad. Sci. USA* **97,** 1079–1084 (2000).
24. Bezrukov, S. M. Ion channels as molecular coulter counters to probe metabolite transport. *J. Membr. Biol.* **174,** 1–13 (2000).
25. Wolf, S. & Tauber, R. N. *Silicon Processing for the VLSI Era* 149–224 (Lattice, Sunset Beach, California, 2000).
26. Rai-Choudhury, P. (ed.) *Handbook of Microlithography, Micromachining, and Microfabrication* 41–97, 153–195 (SPIE-International Society for Optical Engineering, Bellingham, Washington, 1997).
27. Ralls, K. S., Buhrman, R. A. & Tiberio, R. C. Fabrication of thin-film metal nanobridges. *Appl. Phys. Lett.* **55,** 2459–2461 (1989).

Ordered nanoporous arrays of carbon supporting high dispersions of platinum nanoparticles

Sang Hoon Joo*, Seong Jae Choi*, Ilwhan Oh†, Juhyoun Kwak†, Zheng Liu‡, Osamu Terasaki‡§ & Ryong Ryoo*

* *National Creative Research Initiative Center for Functional Nanomaterials and Department of Chemistry, Korea Advanced Institute of Science and Technology, Taejon 305-701, Korea*
† *Electrochemistry Laboratory, Department of Chemistry, Korea Advanced Institute of Science and Technology, Taejon 305-701, Korea*
‡ *CREST, Japan Science and Technology Corporation, Department of Physics, Tohoku University, Sendai 980-8578, Japan*
§ *Department of Physics and Center for Interdisciplinary Research, Tohoku University, Sendai 980-8578, Japan*

Nanostructured carbon materials are potentially of great technological interest for the development of electronic[1,2], catalytic[3,4] and hydrogen-storage systems[5,6]. Here we describe a general strategy for the synthesis of highly ordered, rigid arrays of nanoporous carbon having uniform but tunable diameters (typically 6 nanometres inside and 9 nanometres outside). These structures are formed by using ordered mesoporous silicas as templates, the removal of which leaves a partially ordered graphitic framework. The resulting material supports a high dispersion of platinum nanoparticles, exceeding that of other common microporous carbon materials (such as carbon black, charcoal and activated carbon fibres). The platinum cluster diameter can be controlled to below 3 nanometres, and the high dispersion of these metal clusters gives rise to promising electrocatalytic activity for oxygen reduction, which could prove to be practically relevant for fuel-cell technologies. These nanomaterials can also be prepared in the form of free-standing films by using ordered silica films as the templates.

Various production methods[7] such as arc discharge, laser ablation, chemical vapour deposition, and template synthesis techniques[8] are used to obtain carbon nanotubes in the single-wall, multi-wall or disordered-wall form. In general, during synthesis of the nanotubes, the tube diameters are very difficult to control. The carbon nanotubes are obtained as a powder, with separate or entangled nanotubes that exhibit a broad distribution in tube diameters. Some of the single-wall nanotubes undergo self-organization to a bundle[9]. However, the organization is achieved through weak van der Waals interactions, so that the bundle cannot be considered as a system with rigid structural periodicity. Here we

show that a periodic array of uniform ordered nanoporous carbon can easily be synthesized with tunable pore diameters and rigid structural order (Fig. 1), using the mesoporous aluminosilicate molecular sieves known as SBA-15[10] as templates.

The mesoporous SBA-15 can be produced in a large quantity by the cooperative assembly process which takes place between silica species and the amphiphilic poly(alkylene oxide)-type triblock copolymers in aqueous or organic medium[10]. The SBA-15 silica is constructed with a hexagonal array of nanotubes with uniform diameter. The diameter of the silica tubes can at present be controlled over the range of 6–15 nm depending on synthesis conditions[11]. These tubes are randomly interconnected through complementary pores less than 3.5 nm in diameter. Typically, in our experiments, the SBA-15 silica was synthesized in powder form (particle size of ~1 μm), using tetraethoxysilicon $[Si(C_2H_5O)_4]$ and the $HO(C_2H_4O)_{20}(C_3H_6O)_{70}(C_2H_4O)_{20}H$ triblock copolymer (ref. 10). The resulting SBA-15 silica had cylindrical channels 9 nm in diameter. The SBA-15 silica was converted to an aluminosilicate form with an Si/Al ratio of 20, following the postsynthesis incorporation procedure[12]. The pore volume of the aluminosilicate SBA-15 was filled with furfuryl alcohol ($C_5H_6O_2$) by the incipient-wetness technique. The aluminosilicate SBA-15 containing the furfuryl alcohol was typically heated for 3 h at 80 °C, which resulted in the aluminosilicate acid-catalytic polymerization of the furfuryl alcohol in the form of a layer coated on the pore walls. The remaining furfuryl alcohol without polymerization in the core of the template pores was removed by subsequent evacuation at 80 °C. The polymerized furfuryl alcohol was converted to carbon inside the SBA-15 template by pyrolysis under vacuum while increasing temperatures up to 1,100 °C. The template was then removed with hydrofluoric acid or aqueous NaOH solution. Elemental analysis and energy dispersive X-ray analysis indicated that a negligible amount of silica remained.

The structure of the synthesized carbon is composed of ordered nanoporous carbon, which was originally formed inside the cylindrical nanotubes of the SBA-15 template. Even once the template has been completely removed, the ordered nanoporous carbon is rigidly interconnected into a highly ordered hexagonal array by carbon spacers, which are formed inside the complementary pores between adjacent cylinders. The mesoscopic structural order between the carbon cylinders gives rise to the appearance of more than five Bragg X-ray diffraction (XRD) lines at small scattering angles below $2\theta = 5°$ (Fig. 2a). However, the carbon atoms in the frameworks do not have sufficiently long-range atomic order to exhibit XRD peaks at larger scattering angles. Owing to the short-range atomic order, as in partially ordered graphite, ring patterns and fragmented graphitic lattice fringes appear in the electron diffraction pattern and high-resolution transmission electron micrographs (Fig. 2b). We note that whereas our previous work using sucrose as a carbon source resulted in the formation of rod-type carbons[13,14], the polymerization of furfuryl alcohol by the designed catalytic function of the aluminosilicate frameworks leads to the formation of these pipe-like carbons. The pore-size distribution curve (obtained by the N_2 adsorption isotherm following the Barrett–Joyner–Halenda method with calibration[15]) exhibited two sharp peaks, with the maxima corresponding to the inside diameter of the carbon cylinders (5.9 nm in Fig. 5 of the Supplementary Information) and the pores formed between the adjacent cylinders (4.2 nm), respectively. Here, the outside diameter of the cylinders is controllable by the choice of a template SBA-15 with suitable pore diameter. But the inside diameter, and consequently the wall thickness, is controllable in several ways. One way to do this is by changing the amount of the polymerized furfuryl alcohol using different polymerization temperatures and reaction times. Another way is to add more furfuryl alcohol after the initial polymerization that results in the loss of water.

In such a nanostructured carbon, the pores or channels behave as individual nanoscale reactors so that chemical reactions are confined to take place inside the pores, with only limited diffusion between them. This phenomenon clearly suggests a method of producing nanoscale materials[16]. It also means that nanostructured carbon can be used to support small metal clusters for catalytic[17] and electrocatalytic applications[18]. High metal dispersion (that is, the large fraction of atoms located at the surface of the small metal clusters) is an important design factor for catalysts. High metal dispersion is useful, not only because it saves expensive metal, but also in controlling structure sensitivity (for example, the catalytic selectivity can be changed by decreasing the cluster size). Platinum clusters as small as 1 nm in diameter can be prepared encased in faujasite-type zeolites, and these clusters exhibit high stability up to 400 °C[19]. However, until now, such high metal dispersion combined with stability has been very difficult to obtain with carbons. There are well known methods for producing high Pt dispersions on carbon, but the resulting materials are not used as catalysts because
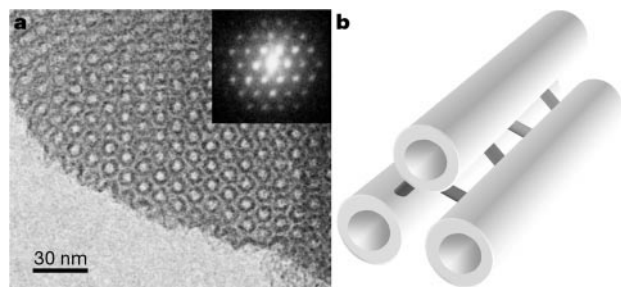

Figure 1 Ordered nanoporous carbon obtained by template synthesis using ordered mesoporous silica SBA-15. **a**, TEM image viewed along the direction of the ordered nanoporous carbon and the corresponding Fourier diffractogram. The image was taken by a JEOL JEM-4000EX instrument (operated at 400 kV). **b**, Schematic model for the carbon structure. The structural model is provided to indicate that the carbon nanopores are rigidly interconnected into a highly ordered hexagonal array by carbon spacers. The outside diameter of the carbon structures is controllable by the choice of a template SBA-15 aluminosilicate with suitable diameter; the inside diameter is controllable by the amount of the carbon source.
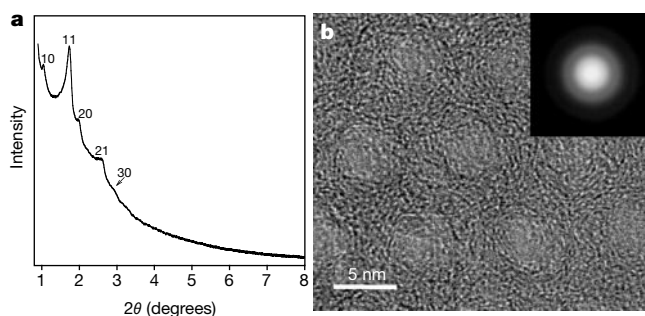

Figure 2 Long-range and short-range order in the structure of ordered nanoporous carbon material. **a**, X-ray diffraction pattern indicating the hexagonal order between carbon cylinders. The XRD pattern was taken by a Rigaku D/MAX-III instrument (operated at 3 kW). The (10) diffraction peak is lower than (11) in intensity, owing to the diffraction interference between the walls and the spacers interconnecting adjacent cylinders. **b**, High-resolution TEM image of carbon cylinders and the corresponding Fourier diffractogram. The image was taken by a JEOL JEM-4000EX instrument (operated at 400 kV). The partially ordered graphitic wall structure not only causes the graphitic lattice fringes to appear in the high-resolution TEM image but also the electron-diffraction ring pattern.

they tend to sinter through Ostwald ripening processes fairly quickly. This difficulty motivated numerous studies to improve metal dispersions on carbons, mainly through optimization of the metal-supporting procedures or functionalization of the carbon surface[17].

However, we found that such small Pt clusters can be prepared very easily by using nanostructured carbon as a support, after a simple incipient-wetness procedure without any surface functionalization. The supported Pt clusters were prepared with an acetone solution of hexachloroplatinic acid (see Methods) and characterized with extended X-ray absorption fine structure (EXAFS), high-resolution TEM and hydrogen chemisorption. The EXAFS result (a Pt–Pt coordination number of 5.4 as shown in Fig. 6 of the Supplementary Information) and the hydrogen chemisorption data (1.5 H atoms per Pt atom) indicate that, when the Pt loading is 2 wt%, the Pt clusters are even smaller than the extremely well dispersed Pt clusters encased in the supercage (1.3 nm in diameter) of NaY zeolites[19]. The cluster size increases with the metal loading, but the extent of the increase is much smaller than for conventional porous carbons. Even when the Pt loading is increased to the same weight of carbon (that is, 50 wt% Pt of the total weight), the Pt clusters show a very narrow particle-size distribution around 2.5 nm (Fig. 3). On the other hand, in the case of other porous carbons such as carbon black, activated charcoal and activated carbon fibre, the same experiments have resulted in the formation of much larger Pt particles with a wide distribution of diameters ranging up to 30 nm.

Nanostructured carbon, capable of supporting Pt clusters with such high and uniform dispersion, may find the most suitable application in fuel cell systems[20] and as hydrophobic catalysts for bulky organic compounds[17]. In fuel cells especially, the high loading of expensive Pt on carbon black has severely limited their widespread use. With this motivation, we compared the electrocatalytic activity of carbon-supported Pt in O_2 reduction with the activities of other carbons, using a rotating-disk electrode. The electrode was prepared by coating 1.5 μg of catalyst (Pt plus carbon) as a thin film onto glassy carbon (see Methods). The electrocatalytic mass activities, that is, the electrocatalytic currents per gram of Pt, were measured at 900 mV with respect to the normal hydrogen electrode, where the reaction can be considered to occur within the kinetic controlled regime[21–23]. The mass activities thus obtained with the 20–50 wt% Pt loadings are much higher than those of the Pt/carbon black samples onto which the Pt particles were supported, using the same procedure as for the ordered nanoporous carbon in the present work (see Fig. 4a). The activity-versus-loading plot for the Pt/nanoporous carbon shows a surprisingly high peak activity amounting to 100 A per g Pt at the 33-wt% Pt loading. Such a high activity indicates that several times higher electrocatalytic currents can be generated using the same amount of Pt in the case of the ordered nanoporous carbon. Other investigations have reported a peak activity ranging from 1.4 to 25 A per g Pt at 900 mV under similar conditions[21–23]. Furthermore, the catalytic current of the Pt ordered nanoporous carbon electrode began to rise much more sharply at a more positive potential, which directly improved the cell efficiency (Fig. 4b). The advantage seemed to come from the uniformity of, and the decrease in, the Pt cluster size when Pt is supported on the nanostructured carbon. Nanostructured carbon with such properties may also be useful for the construction of fuel cell anodes that operate with direct methanol oxidation, where high Pt loading is essential[24].

In addition to the powder form, it is also possible to prepare nanostructured carbon in the form of free-standing thin films by using porous silica films as templates. The carbon films thus synthesized retain the shape of the template films (see Fig. 7 in the Supplementary Information), as well as the hexagonally ordered arrangement of the ordered nanoporous carbon in the same way as in the powder form. The development of nanoporous carbons of such ordered film types may be of great importance in separation technologies using membranes, whereas chemical vapour deposition techniques to prepare carbon films largely fail to produce such highly ordered nanotubes or nanopores. The synthesis technique for carbon may be combined with the recently developed sol–gel methods that are suitable for processing the ordered mesoporous silica templates into the forms of oriented fibres[25] and variously micro-patterned thin films[26,27]. It should also be possible to fabricate micro-bundles of the parallel ordered nanoporous carbon if the mesoporous silica templates can be patterned by micro ink-jet printing[28] of a surfactant containing a silica sol onto the surface of substrates. ☐
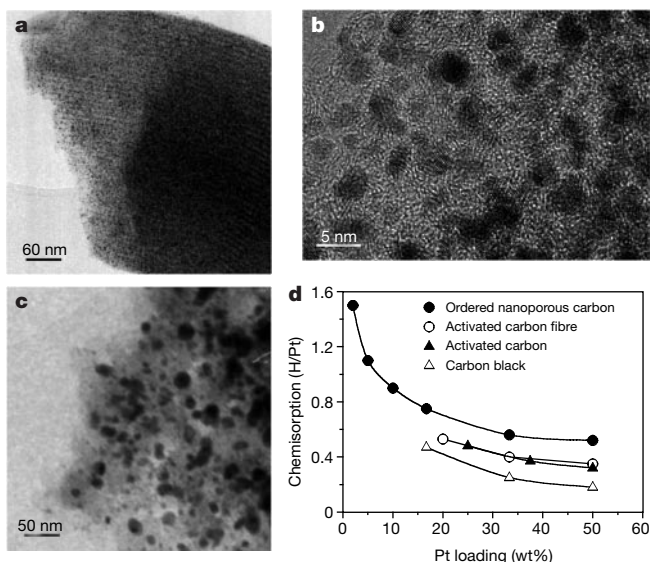

Figure 3 Transmission electron microscope images of the carbon samples supporting the same amount of platinum as the carbon weight. **a**, **b**, Ordered nanoporous carbon with specific surface area 2,000 $m^2 g^{-1}$ as measured by the Brunauer-Emmett-Teller (BET) method; **c**, carbon black (Vulcan XC-72). **d**, Hydrogen chemisorption data (that is, the average number of H atoms chemisorbed per Pt atom) for various kinds of carbons supporting Pt: ordered nanoporous carbon (filled circles), carbon black (empty triangles), activated carbon (Darco KB, BET area = 1,500 $m^2 g^{-1}$) (filled triangle) and activated carbon fibre (Osaka ACF A-15, BET area = 1,500 $m^2 g^{-1}$ (empty circles).
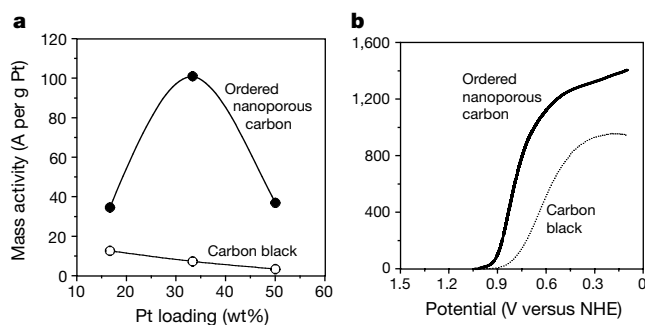

Figure 4 Electrocatalytic mass activities of Pt/carbon catalysts for the O_2 reduction. **a**, Catalytic activity in amperes per gram of Pt measured at a potential of +0.900 V with respect to the normal hydrogen electrode and at a rotating speed of 10,000 r.p.m. in 0.1 M $HClO_4$ saturated with O_2. **b**, The activity–potential relation for 33-wt% Pt/carbons, obtained at 10,000 r.p.m. with a scan rate of 50 mV s^{-1}. The activities were measured on a rotating disk electrode coated with Pt/carbon. The activity of the 33-wt% Pt ordered nanoporous carbon at +0.900 V is 100 ± 16 A per Pt at the 95% confidence level.

letters to nature

Methods

Preparation of Pt clusters, hydrogen chemisorption and EXAFS

One gram of carbon was impregnated with 2 ml acetone containing H_2PtCl_6, drop by drop with vigorous agitation. The amount of H_2PtCl_6 in the solution was varied, depending on the desired metal loading. After being dried in a 60 °C oven, the impregnated carbon sample was heated in a H_2 flow while increasing the temperature from room temperature to 300 °C over 2 h. The sample was subsequently outgassed for 2 h at 300 °C, for the desorption of H_2 from the resultant Pt clusters. Hydrogen adsorption isotherms were measured at room temperature, *in situ* on the Pt clusters, using a volumetric adsorption apparatus. The hydrogen chemisorption (the number of H atoms per Pt atom) was determined by the extrapolation of the adsorption isotherm in the range of 10–30 kPa to zero pressure. For EXAFS, the sample that was outgassed at 300 °C was cooled to room temperature and exposed to air. About 0.1 g of the powder sample was pressed into a disk 10 mm in diameter, using polyethylene powder as a binder, and subsequently treated with H_2 at 80 °C. The EXAFS was measured at the Pt L_{III} edge at room temperature under H_2 atmosphere[26], using the BL 10B facility at the Photon Factory in Tsukuba. Analysis of the EXAFS data was carried out by standard methods using the UWXAFS2 program package as in ref. 19.

Preparation of electrodes and electrocatalytic activity measurements

Twenty milligrams of Pt/C powder and 0.40 ml ethanol containing 5.0 wt% Nafion were ultrasonically dispersed in 100 ml distilled water. A 30-µl portion of the resultant ink was dropped onto an electrode surface, which was composed of a glassy carbon core, 3 mm in diameter; the surrounding insulation area was 6 mm in diameter. The ink was carefully dried in a 70 °C oven so that Pt catalysts could be uniformly coated over the entire cross-section of the 6-mm diameter area. The electrocatalytic current was measured at room temperature and a rotating speed of 10,000 r.p.m., in 0.10 M $HClO_4$ saturated with O_2.

1. Fan, S. *et al.* Self-oriented regular arrays of carbon nanotubes and their field emission properties. *Science* **283**, 512–514 (1999).
2. Rueckes, T. *et al.* Carbon nanotube-based nonvolatile random access memory for molecular computing. *Science* **289**, 94–97 (2000).
3. Planeix, J. M. *et al.* Applications of carbon nanotubes as supports in heterogeneous catalysis. *J. Am. Chem. Soc.* **116**, 7935–7936 (1994).
4. Rodriguez, N. M., Chambers, A. & Baker, R. T. K. Catalytic engineering of carbon nanostructures. *Langmuir* **11**, 3862–3866 (1995).
5. Dillon, A. C. *et al.* Storage of hydrogen in single-walled carbon nanotubes. *Nature* **386**, 377–379 (1997).
6. Lin, J. Hydrogen storage in nanotubes. *Science* **287**, 1929–1929 (2000).
7. Dresselhaus, M. S., Dresselhaus, G. & Eklund, P. C. *Science of Fullerenes and Carbon Nanotubes* (Academic, San Diego, 1996).
8. Kyotani, T., Tsai, L.-F. & Tomita, A. Formation of ultrafine carbon tubes by using an anodic aluminum oxide film as a template. *Chem. Mater.* **7**, 1427–1428 (2000).
9. Thess, A. *et al.* Crystalline ropes of metallic carbon nanotubes. *Science* **273**, 483–487 (1996).
10. Kruk, M., Jaroniec, M., Ko, C. H. & Ryoo, R. Characterization of the porous structure of SBA-15. *Chem. Mater.* **12**, 1961–1968 (2000).
11. Lettow, J. S. *et al.* Hexagonal to mesocellular foam phase transition in polymer-templated mesoporous silicas. *Langmuir* **16**, 8291–8295 (2000).
12. Ryoo, R., Jun, S., Kim, J. M. & Kim, M. J. Generalised route to the preparation of mesoporous metallosilicates via post-synthetic metal implantation. *Chem. Commun.* 2225–2226 (1997).
13. Jun, S. *et al.* Synthesis of new, nanoporous carbon with hexagonally ordered mesostructure. *J. Am. Chem. Soc.* **122**, 10712–10713 (2000).
14. Ryoo, R., Joo, S. H. & Jun, S. Synthesis of highly ordered carbon molecular sieves via template-mediated structural transformation. *J. Phys. Chem. B* **103**, 7743–7746 (1999).
15. Kruk, M., Jaroniec, M. & Sayari, A. Application of large pore MCM-41 molecular sieves to improve pore size analysis using nitrogen adsorption measurements. *Langmuir* **13**, 6267–6273 (1997).
16. Kageyama, K., Tamazawa, J. & Aida, T. Extrusion polymerization: catalyzed synthesis of crystalline linear polyethylene nanofibers within a mesoporous silica. *Science* **285**, 2113–2115 (1999).
17. Radovic, L. R. & Ridriguiz-Reinoso, F. in *Chemistry and Physics of Carbon* Vol. 25 (ed. Thrower, P. A.) 243–358 (Marcel-Dekker, New York, 1997).
18. Kinoshita, K. *Carbon, Electrochemical and Physicochemical Properties* (John Wiley & Sons, New York, 1988).
19. Ryoo, R. *et al.* Application of the xenon-adsorption method for the study of metal cluster formation and growth on Y zeolite. *J. Am. Chem. Soc.* **114**, 76–82 (1992).
20. Kordesch, K. & Simader, G. *Fuel Cells and Their Electrochemistry* (VCH, Weinheim, 1996).
21. Peuckert, M., Yoneda, T., Dalla Betta, R. A. & Boudart, M. Oxygen reduction on small supported platinum particles. *J. Electrochem. Soc.* **133**, 944–947 (1986).
22. Poirier, J. A. & Stoner, G. E. Microstructural effects on electrocatalytic oxygen reduction activity of nano-grained thin-film platinum in acid media. *J. Electrochem. Soc.* **141**, 425–430 (1994).
23. Takasu, Y. *et al.* Size effects of platinum particles on the electroreduction of oxygen. *Electrochim. Acta* **41**, 2595–2600 (1996).
24. Wasmus, S. & Kuver, A. Methanol oxidation and direct methanol fuel cells: a selective review. *J. Electroanal. Chem.* **461**, 14–31 (1999).
25. Yang, P., Zhao, D., Chmelka, B. F. & Stucky, G. D. Triblock-copolymer-directed syntheses of large-pore mesospore silica fibers. *Chem. Mater.* **10**, 2033–2036 (1998).
26. Huang, L. *et al.* Fabrication of ordered porous structures by self-assembly of zeolite nanocrystals. *J. Am. Chem. Soc.* **122**, 3530–3531 (2000).
27. Doshi, D. A. *et al.* Optically, defined multifunctional patterning of photosensitive thin-film silica mesophases. *Science* **290**, 107–111 (2000).
28. Fan, H. Y. *et al.* Rapid prototyping of patterned functional nanostructures. *Nature* **405**, 56–60 (2000).
29. Cho, S. J., Ahn, W.-S., Hong, S. B. & Ryoo, R. Investigation of the platinum cluster size and location on zeolite KL with ^{129}Xe NMR, XAFS, and xenon adsorption. *J. Phys. Chem.* **100**, 4996–5003 (1996).

Supplementary information is available on *Nature*'s World-Wide Web site (http://www.nature.com) or as paper copy from the London editorial office of *Nature*.

Acknowledgements

R.R. thanks M. Nomura for helpful discussions on EXAFS measurement. This work was supported in part by the Ministry of Science and Technology through the Creative Research Initiative Program (R.R.), by the School of Molecular Science through the Brain Korea 21 Project (R.R. and J.K.), by the Korea Science and Engineering Foundation through the MICROS Center at KAIST (J.K.), and by CREST, Japan Science and Technology Corporation (O.T.).

Correspondence and requests for materials should be addressed to R.R.
(e-mail: rryoo@mail.kaist.ac.kr).

The dating of shallow faults in the Earth's crust

Ben A. van der Pluijm*, **Chris M. Hall***, **Peter J. Vrolijk**†, **David R. Pevear**† & **Michael C. Covey**†

* *Department of Geological Sciences, University of Michigan, Ann Arbor, Michigan 48109, USA*
† *ExxonMobil Upstream Research Co., Houston, Texas 77252-2189, USA*

Direct dating of ductile shear zones and calculation of uplift/ exhumation rates can be done using various radiometric dating techniques. But radiometric dating of shallow crustal faulting, which occurs in the crust's brittle regime, has remained difficult[1–4] because the low temperatures typical of shallow crusted faults prevent the complete syntectonic mineral recrystallization that occurs in deeper faults. Both old (detrital) and newly grown (authigenic) fine-grained phyllosilicates are thus preserved in shallow fault zones and therefore their radiometric ages reflect a mixture of both mineral populations. Also, the loss of ^{39}Ar during neutron irradiation in dating of clay minerals can produce erroneously old ages. Here we present a method of characterizing the clay populations in fault gouge, using X-ray modelling, combined with sample encapsulation, and show how it can be used to date near-surface fault activity reliably. We examine fault gouge from the Lewis thrust of the southern Canadian Rockies, which we determine to be ~52 Myr old. This result requires the western North America stress regime to have changed from contraction to extension in only a few million years during the Eocene. We also estimate the uplift/ exhumation age and sedimentary source of these rocks to be ~172 Myr.

Dating of shallow faults is, among other things, critical for our understanding of crustal evolution, plate interaction and fault reactivation, but there are two obstacles to radiometric dating of clay-rich fault rocks: (1) ^{39}Ar recoil in ^{40}Ar/^{39}Ar chronology and (2) 'contamination' of samples from old, detrital material. The momentum transfer that occurs during the ^{39}K(n.p.)→^{39}Ar reaction is sufficient to move a produced Ar atom about 0.1 µm from the site of the original K atom, which, for clay minerals, can be much greater than the average grain thickness. Thus, one expects massive losses of ^{39}Ar during neutron irradiation, which would lead to erroneously old ages. Vacuum-encapsulated irradiation has been developed as a solution to the recoil problem[5–8]. The second problem, a mixed age

172 © 2001 Macmillan Magazines Ltd NATURE | VOL 412 | 12 JULY 2001 | www.nature.com

letters to nature

....

addendum

An efficient room-temperature silicon-based light-emitting diode

Wai Lek Ng, M. A. Lourenço, R. M. Gwilliam, S. Ledain, G. Shao & K. P. Homewood

Nature **410,** 192–194 (2001).

Silicon light-emitting diodes (LED) show light emission at the bandgap energy of silicon with efficiencies approaching those of standard III−V emitters: 0.1% for planar devices (our Letter) and about 1% when total internal reflection is minimized by surface texturing[1]. We point out here an additional example of a silicon device also showing light emission at the bandgap[2]. The authors described devices made by the SACMOS-3 process and focus the bulk of the paper on visible emission under reverse bias. However, they also report briefly on a device operated under forward bias giving efficiencies of around 0.01%, although no explanation of the mechanism is given. It is now becoming clear that crystalline silicon, when appropriately engineered, is capable of supporting efficient light emission, opening up many significant applications. □

1. Green, M. A., Shao, J., Wang, A., Reece, P. J. & Gal, M. Efficient silicon light-emitting diodes. *Nature* **412,** 805–808 (2001).
2. Kramer, J. *et al.* Light-emitting devices in industrial CMOS technology. *Sensors Actuators* **A37−A38,** 527–533 (1993).

....

erratum

Warm tropical sea surface temperatures in the Late Cretaceous and Eocene epochs

Paul N. Pearson, Peter W. Ditchfield, Joyce Singano, Katherine G. Harcourt-Brown, Christopher J. Nicholas, Richard K. Olsson, Nicholas J. Shackleton & Mike A. Hall

Nature **413,** 481–487 (2001).

In this Article, the temperature scale in Figure 3i should have been the same as in Figure 3g. □

....

corrections

Self-assembled monolayer organic field-effect transistors

Jan Hendrik Schön, Hong Meng & Zhenan Bao

Nature **413,** 713–716 (2001).

The values of the transconductance in Table 1 and in the text (page 715, second paragraph) are incorrect. The values should be divided by ten. The data plotted in Figs 2 and 3 are correct and the conclusions are not affected. □

....

Ordered nanoporous arrays of carbon supporting high dispersions of platinum nanoparticles

Sang Hoon Joo, Seong Jae Choi, Ilwhan Oh, Juhyoun Kwak, Zheng Liu, Osamu Terasaki & Ryong Ryoo

Nature **412,** 169–172 (2001).

We inadvertently omitted to cite an earlier reference alongside ref. 8 (G. Che, B. Lakshmi, E. R. Fisher and C. R. Martin *Nature* **393,** 346–349; 1998), which was published in 1995 (and not 2000 as printed). Also, our suggestion that using the pores in a microporous material as templates could be a way in which to produce nanoscale materials has been discussed before (see, for example, C. R. Martin *Science* **266,** 1961–1966 (1994) and J. C. Hulteen & C. R. Martin *J. Mater. Chem.* **7,** 1075−1087 (1997)). □

....

The timing of the last deglaciation in North Atlantic climate records

Claire Waelbroeck, Jean-Claude Duplessy, Elisabeth Michel, Laurent Labeyrie, Didier Paillard & Josette Duprat

Nature **412,** 724–727 (2001).

We directly used the observed leads of sea surface temperature with respect to air temperature (dated in calendar years), whereas the air temperature calendar ages should have been converted into ^{14}C ages, with reservoir ages computed as the difference between marine and atmospheric ^{14}C ages. Taking this into consideration, apparent surface-water ages are $1{,}180 \pm 630$ to $1{,}880 \pm 750$ years at the end of the Heinrich 1 surge event (14,500 years BP) and 930 ± 250 to $1{,}050 \pm 230$ years at the end of the Younger Dryas cold episode. This does not change the discussion and conclusions. □